Differentially synchronized spiking enables multiplexed neural coding

Milad Lankarany[a,b,c,1], Dhekra Al-Basha[a,b], Stéphanie Ratté[a,b,c], and Steven A. Prescott[a,b,c,2]

[a]Neurosciences and Mental Health, The Hospital for Sick Children, Toronto, ON M5G 0A4, Canada; [b]Department of Physiology, University of Toronto, Toronto, ON M5S 1A8, Canada; and [c]Institute of Biomaterials and Biomedical Engineering, University of Toronto, Toronto, ON M5S 3G9, Canada

Edited by Terrence J. Sejnowski, Salk Institute for Biological Studies, La Jolla, CA, and approved April 1, 2019 (received for review July 20, 2018)

Multiplexing refers to the simultaneous encoding of two or more signals. Neurons have been shown to multiplex, but different stimuli require different multiplexing strategies. Whereas the frequency and amplitude of periodic stimuli can be encoded by the timing and rate of the same spikes, natural scenes, which comprise areas over which intensity varies gradually and sparse edges where intensity changes abruptly, require a different multiplexing strategy. Recording in vivo from neurons in primary somatosensory cortex during tactile stimulation, we found that stimulus onset and offset (edges) evoked highly synchronized spiking, whereas other spikes in the same neurons occurred asynchronously. Stimulus intensity modulated the rate of asynchronous spiking, but did not affect the timing of synchronous spikes. From this, we hypothesized that spikes driven by high- and low-contrast stimulus features can be distinguished on the basis of their synchronization, and that differentially synchronized spiking can thus be used to form multiplexed representations. Applying a Bayesian decoding method, we verified that information about high- and low-contrast features can be recovered from an ensemble of model neurons receiving common input. Equally good decoding was achieved by distinguishing synchronous from asynchronous spikes and applying reverse correlation methods separately to each spike type. This result, which we verified with patch clamp recordings in vitro, demonstrates that neurons receiving common input can use the rate of asynchronous spiking to encode the intensity of low-contrast features while using the timing of synchronous spikes to encode the occurrence of high-contrast features. We refer to this strategy as synchrony-division multiplexing.

multiplexing | neural coding | rate code | temporal code | synchrony

The brain processes phenomenal amounts of information despite biological constraints on the number of neurons and their maximal firing rate, plus other factors that limit signal-to-noise ratio (1). Such constraints necessitate efficient neural coding strategies. In telecommunication systems, efficiency is increased by sending multiple messages simultaneously over a single channel. This so-called multiplexing involves representing different messages in separate frequency bands (frequency-division multiplexing) or temporal epochs (time-division multiplexing), among other strategies (2). The brain can also multiplex (3–16), but different stimuli require different multiplexing strategies, many of which have yet to be elucidated.

Ideas about multiplexed neural coding date back nearly a century (17). In auditory nerve, the phase-locking of spikes to a periodic input enables temporal coding of stimulus frequency, whereas the probability of spiking per stimulus cycle (which is <1 when stimulus frequency exceeds the maximal firing rate) enables rate coding of stimulus intensity (18). In this scenario, the same spikes contribute to both codes (*SI Appendix*, Fig. S1*A*), but distinct cochlear nuclei (19) use high- or low-pass filtering to extract either the time- or rate-encoded information. The frequency and intensity of vibrotactile stimuli are similarly encoded by the timing and rate of spikes in somatosensory cortex (3). In these examples, intensity refers to the peak-to-peak amplitude, or envelope, of the periodic stimulus. But not all stimuli are periodic; for instance, natural scenes comprise areas over which intensity varies gradually (low contrast), and sparse edges in which intensity changes abruptly (high contrast) (20). If spikes evoked by low- and high-contrast features are interspersed in a given neuron's spike train, the spikes evoked by each feature must be disambiguated to decode the feature. How might this occur?

High-contrast features tend to evoke spikes whose timing is more precise than spikes evoked by low-contrast features (21–23), but assessing spike-timing precision requires comparison with the stimulus or some other reference (e.g., other spikes). We hypothesized that precisely timed spikes driven by high-contrast features occur synchronously across neurons receiving common input, whereas other spikes driven by low-contrast features occur asynchronously. If different stimulus features evoke differentially synchronized spiking, information about each feature could be recovered from each spike "type." In this scenario, unlike for multiplexed coding of periodic stimuli, the representation of each feature is based on separate (synchronous vs. asynchronous) spikes that occur in the same neurons (*SI Appendix*, Fig. S1*B*). Other scenarios are also possible; for instance, where synchronous and asynchronous spikes occur in different neurons (*SI Appendix*, Fig. S1*C*). The appropriate multiplexing strategy ultimately depends on the stimulus.

Starting with in vivo recordings from somatosensory cortex, we confirmed that the onset and offset of tactile stimuli (high-contrast

Significance

The nervous system processes phenomenal amounts of information. This processing must be conducted efficiently. In telecommunications systems, efficiency is increased by transmitting multiple signals through a single communication channel, or multiplexing. Neurons also multiplex. Here, we demonstrate a strategy for multiplexing different features of aperiodic stimuli: Cortical neurons use the rate of asynchronous spiking to encode stimulus intensity while using the timing of synchronous spikes to encode abrupt changes in stimulus intensity. This is possible because high-contrast features (e.g., edges) evoke spikes that transiently synchronize across neurons, whereas low-contrast features evoke sustained asynchronous spiking whose rate is proportional to stimulus intensity. Differentially synchronized spiking evoked in the same neurons by different stimulus features enables the formation of multiplexed representations.

Author contributions: M.L. and S.A.P. designed research; M.L., D.A.-B., and S.R. performed research; M.L., D.A.-B., S.R., and S.A.P. analyzed data; and M.L., D.A.-B., S.R., and S.A.P. wrote the paper.

The authors declare no conflict of interest.

This article is a PNAS Direct Submission.

[1]Present address: Krembil Research Institute, University Health Network, Toronto, ON M5T 0S8, Canada.

[2]To whom correspondence should be addressed. Email: steve.prescott@sickkids.ca.

This article contains supporting information online at www.pnas.org/lookup/suppl/doi:10.1073/pnas.1812171116/-/DCSupplemental.

Published online April 26, 2019.

features) evoked transiently synchronized spiking, whereas intervening spikes occurred asynchronously. The rate of asynchronous spiking varied with the intensity of sustained tactile input (a low-contrast feature). In other words, the rate of asynchronous spiking encoded stimulus intensity, whereas the timing of synchronous spikes encoded high-contrast edges. In subsequent simulations and in vitro recordings, we verified the importance of distinguishing between synchronous and asynchronous spikes to recover information about stimulus intensity and contrast.

Results

Rate and Temporal Coding of Tactile Information in Primary Somatosensory (S1) Cortex. To explore how the different aspects of tactile stimulation are encoded in S1 cortex, we recorded single units in vivo (Fig. 1*A*) while applying steps of increasing force to the whisker pad of lightly sedated rats. Sedation facilitated reproducible stimulation while avoiding the altered sensory processing caused by anesthesia (24). Firing rate histograms (FRHs) were calculated using a broad or narrow kernel to, respectively, track slow or fast changes in firing rate (25). The high-resolution FRH (in black) exhibited distinctive blips that, when appropriately thresholded, predict stimulus onset and offset with near-perfect sensitivity and specificity (Fig. 1*B*). These blips coincided with large negativities in the local field potential (Fig. 1*C*). An expanded view of the rasters (Fig. 1*D*) reveals that firing rate blips result from a volley of synchronous spikes; some neurons produce a rapid burst of two to four spikes, but most contribute a single spike to each volley. All spikes occurring while the high-resolution FRH exceeded threshold (red shading) were designated as synchronous and colored red; all other spikes were designated as asynchronous and colored blue.

The latency of synchronous spikes was insensitive to stimulus intensity (Fig. 1*E*), whereas the rate of asynchronous spiking correlated with stimulus intensity (Fig. 1*F*). Consistent with our hypothesis, these data argue that abrupt changes in stimulus intensity (i.e., high-contrast edges) are encoded by the transient synchronization of spiking, whereas intensity is encoded by the rate of asynchronous spiking. One may have expected synchronous and asynchronous spikes to be segregated to different neurons, as occurs upstream, but our data clearly show synchronous and asynchronous spikes interspersed in the same neurons.

An Ensemble of Neurons Receiving Common Fast and Slow Signals Can Multiplex. The ability of cortical neurons to multiplex using differentially synchronized spiking raises the issue of what inputs they receive. In particular, we must ask how stimulus intensity (a first-order feature) and changes in intensity, or contrast (a second-order feature), are represented in primary sensory neurons, as it is the output of these neurons that eventually becomes the input to cortical neurons. Similar to image compression algorithms that decompose scenes according to first- and second-order features (26), retinal ganglion neurons (27), somatosensory

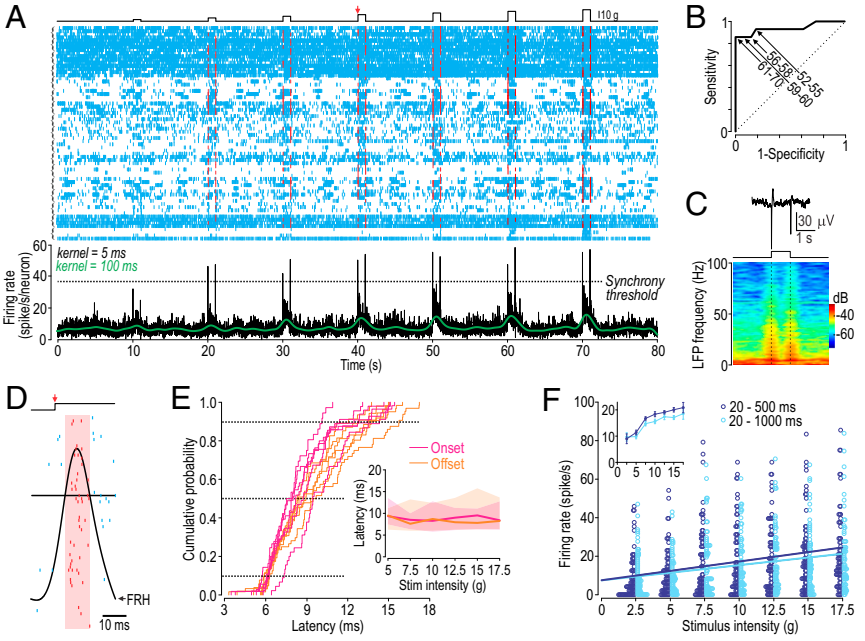

Fig. 1. Neurons in primary somatosensory (S1) cortex use spike timing and rate to encode different tactile stimulus features. (*A*) Rasters from 17 neurons, four trials each, during tactile simulation (*Top*). FRH was calculated using a narrow (σ = 5 ms; black) or broad (σ = 100 ms; green) Gaussian kernel. Black FRH was thresholded to distinguish synchronous (red) from asynchronous (blue) spikes. Arrow highlights 10 g stimulus. (*B*) Receiver operating characteristic curve shows sensitivity and specificity with which synchronized spiking can predict stimulus onset or offset, depending on threshold value. Numbers on graph show threshold as percentage of maximum possible firing rate. Synchrony threshold = 65% for *A* and *D*, which means the onset and offset of the weakest stimulus (2.5 g) was not detected. If only stimuli ≤10 g are considered, 100% sensitivity and 86% specificity can be achieved by lowering the threshold. (*C*) Local field potential (LFP) averaged across five responses to 10 g stimulation (*Top*) and the corresponding spectrogram (*Bottom*). (*D*) Horizontally expanded rasters at onset of 10 g stimulus. Spikes during interval when FRH exceeds synchrony threshold (red shading) are considered synchronous. Some cells produce a quick burst of two to four spikes, but most contribute a single spike per volley. All true positive synchronized volleys (i.e., those that correctly identify stimulus onset or offset) are complete within 20 ms. (*E*) Cumulative probability distribution of synchronous spike latency from stimulus onset (*pink*) or offset (*orange*). Each curve represents a different stimulus intensity. (*Inset*) Median latency (lines) and 10–90 percentile range (shading) do not vary systematically with stimulus intensity. (*F*) Modulation of sustained firing rate. Excluding the first 20 ms, during which synchronous spikes occur; firing rate was calculated over the first half (20–500 ms, *blue*) or full duration (20–1,000 ms, *cyan*) of each stimulus step to gauge the effects of adaptation. Regression line slopes differed significantly from horizontal ($P < 0.0001$, one-sample t tests). (*Inset*) Average rate of 17 neurons averaged across trials to give mean ± SEM. Firing rate was significantly affected by stimulus intensity ($F_{6,42} = 21.42$; $P < 0.001$, two-way ANOVA) and adaptation ($F_{1,42} = 7.22$; $P = 0.01$); firing rate evoked by 2.5 or 5 g was consistently less than that evoked by ≥7.5 g ($P < 0.05$, Student-Neuman-Keuls post hoc tests).

afferents (28), vestibular afferents (29), and electrosensory afferents of the electric fish (30) all exhibit dichotomous tuning: Neurons behaving as low-pass filters (integrators) encode stimulus intensity, whereas others behaving as high-pass filters (coincidence detectors, edge detectors) are sensitive to contrast (31). Differently tuned sensory neurons are coactivated by natural stimuli, which comprise independent first- and second-order features (20), yet each neuron type responds to (encodes) different stimulus features, meaning each feature is initially encoded by distinct sets of sensory afferents (Fig. 2*A* and *SI Appendix*, Fig. S2). Retinal ganglion cells sensitive to luminance or contrast, respectively, follow the parvocellular and magnocellular pathways to the brain (32), but those pathways at least partially reconverge (33–36). Distinctly tuned somatosensory (37, 38), vestibular (29), and auditory pathways (19) similarly reconverge. Central representations tend to expand rather than contract, and although convergence can lead to representations being deliberately transformed through computations, data in Fig. 1 show that information initially conveyed by segregated pathways comes to be represented using different spike types in common cortical neurons.

Because only multiplexed representations can be demultiplexed, we tested whether multiplexing occurs by testing whether slow and fast signals, reflecting the activity evoked by low- and high-contrast features in integrators and coincidence detectors, respectively, can both be recovered (demultiplexed) from the spiking evoked by a mixed signal (Fig. 2*B*). Specifically, we compared standard reverse correlation and Bayesian decoding methods applied to simulated responses from a single neuron or from a 30-neuron ensemble (*SI Appendix*); spikes were not subdivided into different "types" for this initial analysis. The slow signal was recovered from the single-neuron and ensemble responses using either decoding strategy, but the fast signal was recovered only from the ensemble response, and only with the Bayesian method (Fig. 2*C*). These results show that multiplexing can occur, but that it requires a multineuron representation, consistent with the hypothesized role of synchrony for disambiguating spikes driven by different stimulus features.

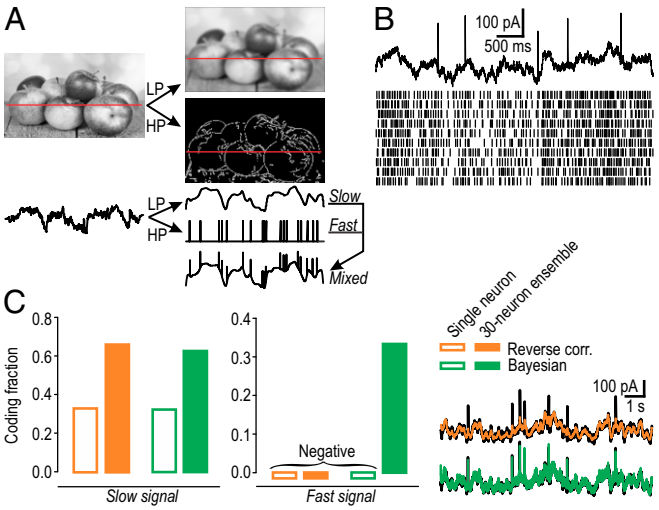

Fig. 2. Slow and fast signals can be demultiplexed from responses to mixed signal. (*A*) Basis for mixed signal. (*A*, *Top*) Decomposition of image by sensory neurons behaving as low-pass (LP) or high-pass (HP) filters. (*A*, *Bottom*) Gray-scale intensity along cut through LP image corresponds to slow signal representing luminance, a first-order stimulus feature. Same cut through HP image yields a series of discrete events representing edges and other areas of high contrast, a second-order stimulus feature. Convergence of those signals creates a "mixed" signal. See also *SI Appendix*, Fig. S2. (*B*) Sample rasters from 10 model neurons (*Bottom*) receiving a common mixed signal (*Top*) and independent noise (not illustrated). Spiking evoked by the fast component is not obviously different from spiking evoked by the slow component. (*C*) Decoding of the mixed signal using standard reverse correlation (orange) or a Bayesian decoding method (green) applied to the response of a single neuron (open bars) or a 30-neuron ensemble (filled bars). (*Inset*) Original mixed signal (black) overlaid with signal reconstructed from the ensemble response (color; *Methods* and *SI Appendix*, Fig. S3). Signal reconstruction was quantified as coding fraction, $CF = 1 - \frac{\|original - reconstructed\|_2}{\|original\|_2}$, where CF = 1 represents perfect reconstruction and CF ≤ 0 represents failure to explain any variance.

Differentially Synchronized Spiking Enables the Formation of Multiplexed Representations. Guided by results in Fig. 1, we reanalyzed data in Fig. 2 after separating synchronous and asynchronous spikes. In Fig. 3*A*, the low-resolution FRH (shown in green) shows rate fluctuations that track the intensity of the slow signal, whereas the high-resolution FRH (shown in black) exhibits blips representing synchronous spikes that coincide with events in the fast signal. The high-resolution FRH was thresholded to separate synchronous spikes (shown in red) from asynchronous spikes (shown in blue). Pairwise cross-correlograms (CCGs) constructed from each spike type are distinct (Fig. 3*B*), and their superposition explains CCGs with a broad base and narrow peak (*Discussion*).

If each spike type is driven by a different component of the mixed signal, the spike-triggered average (STA) calculated from the mixed signal should be distinct for each spike type. Consistent with slow and fast signals driving asynchronous and synchronous spikes, respectively, the STA calculated from the slow signal using asynchronous spikes (STA^{slow}_{async}) was broad, whereas the STA calculated from the fast signal using synchronous spikes (STA^{fast}_{sync}) was narrow (Fig. 3*C*, dark blue and red STAs). Access to component signals is unnecessary, as similar STAs were recovered from the mixed signal, using asynchronous or synchronous spikes (pale-colored STAs). Consistent with the slow signal not driving synchronous spikes and the fast signal not driving asynchronous spikes, STA^{slow}_{sync} and STA^{fast}_{async} were unstructured (gray STAs). Given that STAs are differently shaped depending on which spike type is used for triggering, we reasoned that reverse correlation could be improved by convolving each spike type with its respective STA, rather than convolving all spikes with STA_{all}. As expected, the fast signal was recovered by convolving synchronous spikes with STA^{fast}_{sync} or STA^{mixed}_{sync}, and the slow signal was recovered by convolving asynchronous spikes with STA^{slow}_{async} or STA^{mixed}_{async} (Fig. 3*C*, *Bottom*). This decoding strategy, which we term synchrony-based demultiplexing, matched the performance of Bayesian decoding (Fig. 3*D*). Failure of Bayesian decoding to recover the fast signal when the encoding model was prevented from learning the fast signal (Fig. 3*D*, light green and *SI Appendix*) confirms that identifying each spike type is necessary for the Bayesian model's performance. In short, separating synchronous and asynchronous spikes is necessary and sufficient for demultiplexing under the conditions tested.

For synchrony-based demultiplexing to occur in the brain, a biologically implementable decoder must be able to distinguish between synchronous and asynchronous spikes. This is readily achieved through high- or low-pass filtering (Fig. 3*E*), which can be implemented by cellular (31), synaptic (39), or microcircuit (40) mechanisms. Our data do not demonstrate how or where demultiplexing occurs, but the observation that spike timing and rate both contribute to tactile perception (4) argues that it must occur if the underlying representations in S1 cortex are multiplexed, as shown in Fig. 1.

Synchrony-Division Multiplexing Is Feasible in Cortical Pyramidal Neurons. To test the feasibility of synchrony-division multiplexing in real neurons, we used whole-cell patch clamp to stimulate and

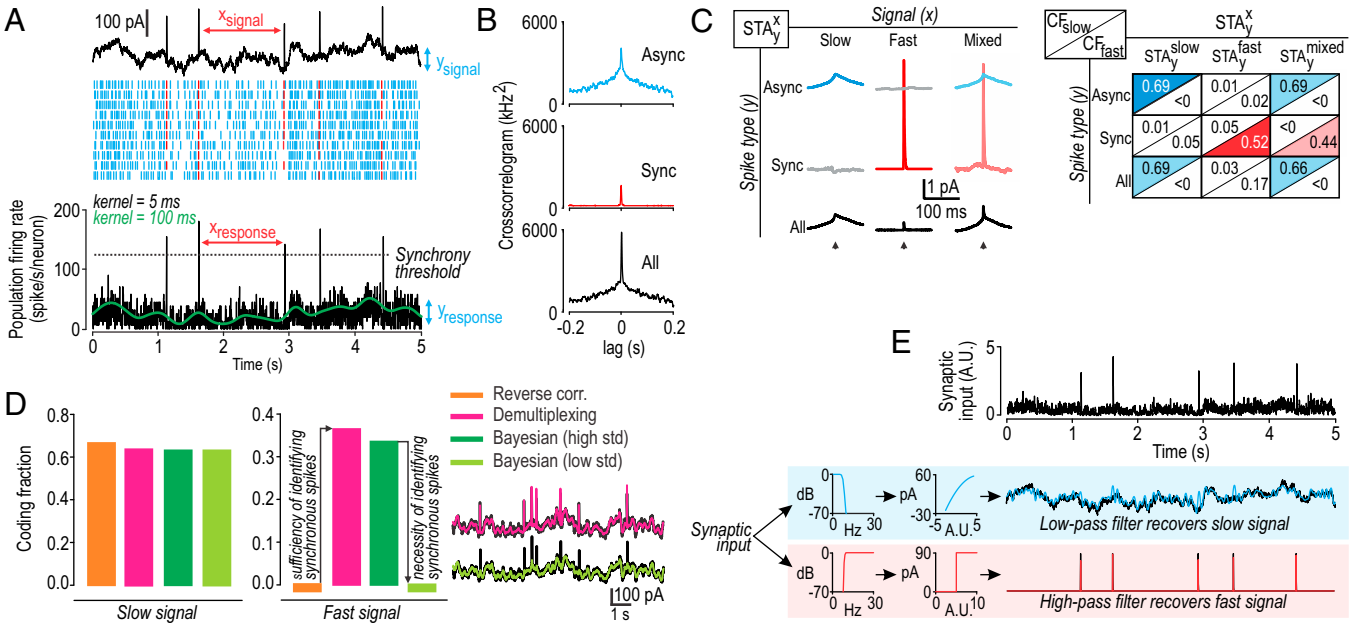

Fig. 3. Differentially synchronized spiking enables multiplexed coding of slow and fast signals. (*A*) Same rasters as in Fig. 2*B* with FRHs constructed with a narrow ($\sigma = 5$ ms; black) or broad ($\sigma = 100$ ms; green) Gaussian kernel. Slow fluctuations in the green FRH track the slow signal, whereas blips in the black FRH coincide with events in the fast signal. Black FRH was thresholded to distinguish synchronous (red) from asynchronous (blue) spikes. Arrows highlight values whose distributions are shown in *SI Appendix*, Fig. S4. (*B*) Pairwise cross-correlograms (CCGs) constructed from asynchronous spikes are broad (*Top*) whereas those constructed from synchronous spikes are narrow (*Middle*), consistent with rate comodulation and precise spike time synchronization driven by the common slow and fast signals, respectively (*SI Appendix*, Fig. S5). (*C*, *Left*) Spike-triggered averages (STA_y^x) were calculated from the fast, slow, or mixed signal (identified as x) using asynchronous, synchronous, or all spikes (identified as y). STA_{sync}^{slow} and STA_{async}^{fast} (gray) were both unstructured, consistent with the slow signal not driving synchronous spikes and the fast signal not driving asynchronous spikes. Conversely, STA_{async}^{slow} (dark blue) and STA_{sync}^{fast} (dark red) are consistent with the slow signal driving asynchronous spikes and the fast signal driving synchronous spikes. Similar STAs were recovered from the mixed signal, depending on the spike type (pale colors). (*C*, *Right*) Reverse correlation based on convolving each spike type with each STA type. Conditions yielding good reconstructions (high CF values) are highlighted in color. (*D*) Decoding of the mixed signal from the ensemble response. Synchrony-based demultiplexing (*pink*) matched the performance of the Bayesian method (*dark green*). Preventing the encoding model used for the Bayesian method from learning to fit rapid rate fluctuations degraded performance (*light green*). (*E*) Demultiplexing. Spikes from conductance based models in *A* were convolved with a synaptic waveform ($\tau_{rise} = 0.5$ ms; $\tau_{decay} = 3$ ms) and summed to provide synaptic input (in arbitrary units, A.U.) to postsynaptic firing rate models that comprise a low- or high-pass filter. Model output (color) is overlaid on the original fast or slow signals (black). Integrator-type model (blue) extracted the slow signal whereas the coincidence detector-type model (red) extracted the fast signal from the multiplexed representations encoded by conductance based models.

record pyramidal neurons in a slice preparation of mouse S1 cortex. A noisy, high-conductance state (41) was recreated using dynamic clamp; conductance noise was different for each neuron and each trial, whereas the mixed signal was the same for all neurons and all trials, as in simulations. Neurons were recorded sequentially, but responses were aligned on the basis of the common mixed signal. As expected, synchronous spikes coincided with events in the fast signal, whereas the rate of asynchronous spiking tracked intensity of the slow signal (Fig. 4*A*). The same decoding strategies applied to simulation data yielded comparable results when applied to these experimental data (Fig. 4*B*). Additional testing of neurons in a noisy, low-conductance state (Fig. 4*C*) or without any added noise (Fig. 4*D*) yielded similar results, indicating that synchrony-division multiplexing is feasible across a broad range of conditions.

Discussion

Our results demonstrate that small ensembles of cortical neurons can multiplex by using the rate of asynchronous spikes to encode stimulus intensity and the timing of synchronous spikes to encode high-contrast features such as edges. We refer to this as synchrony-division multiplexing because different stimulus features are represented by spikes that are differentiated by their degree of synchrony, as opposed to being represented in different frequency bands or temporal epochs (as in frequency- or time-division multiplexing). Importantly, synchronous and asynchronous spikes occur in the same cortical neurons, which is unlike the segregated representation of intensity and contrast across dichotomously tuned primary sensory neurons (28).

To the best of our knowledge, this is the first time multiplexing on the basis of differentially synchronized spiking in the same neurons has been described, although the nervous system has been shown to use other multiplexing strategies. For instance, the rate and timing of spikes in auditory afferents have been shown to respectively encode stimulus intensity and frequency (18), and cochlear nuclei are known to demultiplex those representations (19). We have not demonstrated whether or how multiplexed representation in S1 neurons are demultiplexed, but simple high- or low-pass filtering similar to processing carried out in the cochlear nuclei would suffice (Fig. 3*E*). Demultiplexing is likely to occur, given that tactile perception depends on both the timing and rate of spikes in S1 neurons (4). Indeed, there is extensive work showing that spike timing and rate both carry information about tactile input. Our results do not contradict those findings but, rather, help reconcile them by revealing how different coding schemes can coexist. It is easy to overlook synchrony-division multiplexing by testing with simple stimuli, measuring only certain aspects of a multifaceted response, or neglecting what happens in neighboring neurons, but it is important to recognize that different spikes within the same spike train may encode different information.

Information about the intensity and frequency of a periodic signal such as sound (17, 18) or vibrotactile input (3) is carried by the same spikes, unlike in synchrony-division multiplexing, where

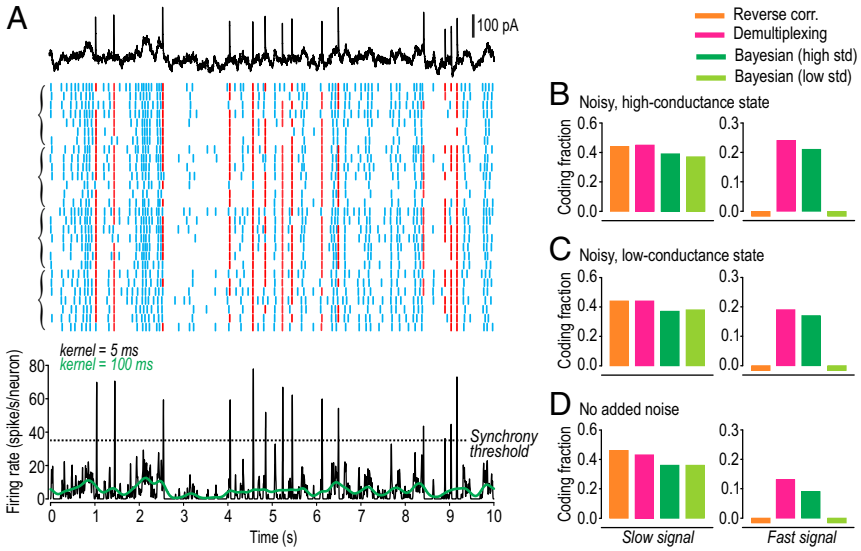

Fig. 4. Pyramidal neurons can multiplex in vitro. (*A*) Sample rasters from short length of 100-s-long responses. All neurons received the same mixed signal but different conductance noise on each trial. Four neurons were tested with 7 trials each; brackets on left group responses by neuron. Black FRH was thresholded to identify synchronous (red) or asynchronous (blue) spikes. (*B*) Decoding of the mixed signal from ensemble response (28 trials) illustrated in *A*, based on neurons tested in the noisy, high-conductance state. Same analysis conducted on neurons tested in a noisy, low-conductance state (31 trials from six neurons) (*C*) or in neurons without any added noise (29 trials from five neurons) (*D*). For all different conditions, the four decoding strategies yielded a pattern of CF values very similar to that seen in simulations (Fig. 3*D*).

separate spikes encode each stimulus feature (*SI Appendix*, Fig. S1). The latter strategy is necessary when high-contrast features occur irregularly, in which case the absolute timing of such features rather than the interval between them is key; moreover, intensity does not refer to the amplitude (envelope) of a recurring high-contrast feature but, rather, to the intensity of interspersed low-contrast features. Encoding interspersed low- and high-contrast features rather than the frequency and amplitude of a more homogeneous, high-frequency signal requires representations that comprise separate spikes. In theory, spike "types" might be distinguished in different ways: by their patterning within a neuron (42, 43), their differential association with network oscillations (7, 44), or their stimulus-induced correlation across neurons (10, 16, 45). The coexistence of correlations with distinct timescales, evidenced by CCGs with a broad base and narrow peak (e.g., refs. 15, 46, and 47), points to simultaneous rate co-modulation and spike-time synchronization (48–50). Similar CCGs are produced by the intermittently synchronized spiking evoked by stimuli tested here (Fig. 3*B*). We distinguished synchronous from asynchronous spikes by thresholding the FRH (Fig. 1 *A* and *B*), but similar classification is possible by cross-referencing spikes to the local field potential (Fig. 1*C*), as in Hong et al. (10), or by identifying "surplus" synchrony in other ways (48, 50).

In conclusion, synchrony-division multiplexing describes a way in which information about different stimulus features can be encoded by different spikes occurring in the same neuron. The key to extracting information about each stimulus feature is to recognize which spikes were driven by which feature. For natural visual or tactile scenes comprising areas of low contrast interspersed with sparse high-contrast edges, the differentially synchronized spiking evoked by those stimulus features provides the means to recognize which feature evoked which spikes. Simple filtering by synaptic or intrinsic cellular mechanisms (Fig. 3*E*) is sufficient to extract one or the other signal. Indeed, reverse correlation methods suffice to recover multiple signals so long as spike types are appropriately discriminated. Synchrony-division multiplexing adds to a growing list of multiplexing strategies, the diversity of which reflects the diverse signals the nervous system must efficiently process.

Materials and Methods

All procedures were approved by the Animal Care Committee of The Hospital for Sick Children. Responses of single units to tactile stimulation of the whisker pad were recorded from S1 cortex of five rats lightly sedated with fentanyl. In separate patch clamp recordings, responses to mixed signals applied through the recording pipette were recorded from layer 5 pyramidal neurons in mouse brain slices. Conductance-based neuron models were simulated using Morris-Lecar equations. See *SI Appendix* for details. Experimental data and code for simulations and analysis are available from prescottlab.ca.

Reverse Correlation. Spikes were passed through a linear filter to reconstruct the signal that evoked them. The filter used here was the STA. The STA kernel was calculated (using training data) by averaging the signal x over a certain time window (kernel width = 50 ms) preceding each spike (51). The reconstructed signal was obtained by convolving spikes (using test data) with the STA kernel

$$S_{\text{est}} = R_{\text{obs}}(t) * STA^{x}_{R_{\text{obs}}}(t) = \int R_{\text{obs}}(q) STA^{x}_{R_{\text{obs}}}(t-q)\mathrm{d}q, \qquad [1]$$

where S_{est} is the estimated signal and R_{obs} is the observed response, which includes all spikes for standard reverse correlation but only specific spike types for demultiplexing as described under *Synchrony-Based Demultiplexing*.

Synchrony-Based Demultiplexing. By using different spike types (y) as the trigger and drawing the spike-triggered ensemble from different components of the signal (x), we calculated STA variants, denoted STA^{x}_{y}. Reverse correlation was carried out as described earlier, but now R_{obs} comprising only specific spike types was convolved with the respective STA to reconstruct each component signal, which were then summed to reconstruct the mixed signal.

Bayesian Decoding. Given an encoding model (*SI Appendix*), we applied a Bayesian strategy to estimate the most likely input given an observed output. The rate-based encoding model was fit to the firing rate observed in a conductance-based model neuron or ensemble thereof during stimulation with I_{mixed} and I_{noise}.

Quantification of Signal Reconstruction. Reconstruction of the original signal was quantified as coding fraction (CF) (52) and is equivalent to variation accounted for (16), where

$$CF = 1 - \frac{\|original - reconstructed\|_2}{\|original\|_2}, \quad [2]$$

and $||.||_2$ indicates the norm 2. CF lies within [−1, 1], where 1 represents perfect reconstruction. Negative values occur when the SD of the difference between original and reconstructed signals is larger than that of the original signal, but are reported here simply as <0. See *SI Appendix* for further details.

ACKNOWLEDGMENTS. We thank Dan Simons and Taro Toyoizumi for feedback on the manuscript, Dan Simons for advice on in vivo experimental procedures, and Russell Smith for expert technical assistance. This study was supported by NIH Grant R01 NS076706 and a Discovery Grant from the Natural Sciences and Engineering Research Council of Canada. M.L. was supported by a Fonds de recherhe du Québec–Santé fellowship, D.A.-B. was supported by an Ontario Graduate Scholarship and Restracomp studentship, and S.A.P. was supported by a Canadian Institutes of Health Research New Investigator Award.

1. Laughlin SB, Sejnowski TJ (2003) Communication in neuronal networks. *Science* 301: 1870–1874.
2. Lathi BP, Ding Z (2009) *Modern Digital and Analog Communication Systems* (Oxford Univ Press, New York), 4th Ed.
3. Harvey MA, Saal HP, Dammann JF, 3rd, Bensmaia SJ (2013) Multiplexing stimulus information through rate and temporal codes in primate somatosensory cortex. *PLoS Biol* 11:e1001558.
4. Zuo Y, et al. (2015) Complementary contributions of spike timing and spike rate to perceptual decisions in rat S1 and S2 cortex. *Curr Biol* 25:357–363.
5. Blumhagen F, et al. (2011) Neuronal filtering of multiplexed odour representations. *Nature* 479:493–498.
6. Masuda N (2006) Simultaneous rate-synchrony codes in populations of spiking neurons. *Neural Comput* 18:45–59.
7. Akam T, Kullmann DM (2014) Oscillatory multiplexing of population codes for selective communication in the mammalian brain. *Nat Rev Neurosci* 15:111–122.
8. Koepsell K, et al. (2009) Retinal oscillations carry visual information to cortex. *Front Syst Neurosci* 3:4.
9. Pirschel F, Kretzberg J (2016) Multiplexed population coding of stimulus properties by leech mechanosensory cells. *J Neurosci* 36:3636–3647.
10. Hong S, et al. (2016) Multiplexed coding by cerebellar Purkinje neurons. *eLife* 5: e13810.
11. Riehle A, Grün S, Diesmann M, Aertsen A (1997) Spike synchronization and rate modulation differentially involved in motor cortical function. *Science* 278:1950–1953.
12. Biederlack J, et al. (2006) Brightness induction: Rate enhancement and neuronal synchronization as complementary codes. *Neuron* 52:1073–1083.
13. Friedrich RW, Habermann CJ, Laurent G (2004) Multiplexing using synchrony in the zebrafish olfactory bulb. *Nat Neurosci* 7:862–871.
14. Isett BR, Feasel SH, Lane MA, Feldman DE (2018) Slip-based coding of local shape and texture in mouse S1. *Neuron* 97:418–433.e5.
15. Dan Y, Alonso JM, Usrey WM, Reid RC (1998) Coding of visual information by precisely correlated spikes in the lateral geniculate nucleus. *Nat Neurosci* 1:501–507.
16. Metzen MG, et al. (2015) Coding of envelopes by correlated but not single-neuron activity requires neural variability. *Proc Natl Acad Sci USA* 112:4791–4796.
17. Wever E, Bray C (1930) Present possibilities for auditory theory. *Psychol Rev* 37: 365–380.
18. Johnson DH (1980) The relationship between spike rate and synchrony in responses of auditory-nerve fibers to single tones. *J Acoust Soc Am* 68:1115–1122.
19. Sullivan WE, Konishi M (1984) Segregation of stimulus phase and intensity coding in the cochlear nucleus of the barn owl. *J Neurosci* 4:1787–1799.
20. Simoncelli EP, Olshausen BA (2001) Natural image statistics and neural representation. *Annu Rev Neurosci* 24:1193–1216.
21. Mainen ZF, Sejnowski TJ (1995) Reliability of spike timing in neocortical neurons. *Science* 268:1503–1506.
22. Berry MJ, Warland DK, Meister M (1997) The structure and precision of retinal spike trains. *Proc Natl Acad Sci USA* 94:5411–5416.
23. Buracas GT, Zador AM, DeWeese MR, Albright TD (1998) Efficient discrimination of temporal patterns by motion-sensitive neurons in primate visual cortex. *Neuron* 20: 959–969.
24. Constantinople CM, Bruno RM (2011) Effects and mechanisms of wakefulness on local cortical networks. *Neuron* 69:1061–1068.
25. Shimazaki H, Shinomoto S (2010) Kernel bandwidth optimization in spike rate estimation. *J Comput Neurosci* 29:171–182.
26. Desai UY, Mizuki MM, Masaki I, Horn BKP (1996) Edge and mean based image compression (Massachusetts Institute of Technology Artificial Intelligence Lab, Cambridge, MA), Technical Report A.I. Memo 1584.
27. Zeck GM, Xiao Q, Masland RH (2005) The spatial filtering properties of local edge detectors and brisk-sustained retinal ganglion cells. *Eur J Neurosci* 22:2016–2026.
28. Johnson KO (2001) The roles and functions of cutaneous mechanoreceptors. *Curr Opin Neurobiol* 11:455–461.
29. Curthoys IS, MacDougall HG, Vidal PP, de Waele C (2017) Sustained and transient vestibular systems: A physiological basis for interpreting vestibular function. *Front Neurol* 8:117.
30. Suga N (1967) Coding in tuberous and ampullary organs of a gymnotid electric fish. *J Comp Neurol* 131:437–452.
31. Ratté S, Lankarany M, Rho YA, Patterson A, Prescott SA (2015) Subthreshold membrane currents confer distinct tuning properties that enable neurons to encode the integral or derivative of their input. *Front Cell Neurosci* 8:452.
32. Lennie P (1980) Parallel visual pathways: A review. *Vision Res* 20:561–594.
33. Dreher B, Wang C, Burke W (1996) Limits of parallel processing: Excitatory convergence of different information channels on single neurons in striate and extrastriate visual cortices. *Clin Exp Pharmacol Physiol* 23:913–925.
34. Sawatari A, Callaway EM (1996) Convergence of magno- and parvocellular pathways in layer 4B of macaque primary visual cortex. *Nature* 380:442–446.
35. Vidyasagar TR, Kulikowski JJ, Lipnicki DM, Dreher B (2002) Convergence of parvocellular and magnocellular information channels in the primary visual cortex of the macaque. *Eur J Neurosci* 16:945–956.
36. Nealey TA, Maunsell JH (1994) Magnocellular and parvocellular contributions to the responses of neurons in macaque striate cortex. *J Neurosci* 14:2069–2079.
37. Saal HP, Bensmaia SJ (2014) Touch is a team effort: Interplay of submodalities in cutaneous sensibility. *Trends Neurosci* 37:689–697.
38. Saal HP, Harvey MA, Bensmaia SJ (2015) Rate and timing of cortical responses driven by separate sensory channels. *eLife* 4:e10450.
39. Middleton JW, Longtin A, Benda J, Maler L (2006) The cellular basis for parallel neural transmission of a high-frequency stimulus and its low-frequency envelope. *Proc Natl Acad Sci USA* 103:14596–14601.
40. Patel M, Joshi B (2013) Decoding synchronized oscillations within the brain: Phase-delayed inhibition provides a robust mechanism for creating a sharp synchrony filter. *J Theor Biol* 334:13–25.
41. Destexhe A, Rudolph M, Paré D (2003) The high-conductance state of neocortical neurons in vivo. *Nat Rev Neurosci* 4:739–751.
42. Mease RA, Kuner T, Fairhall AL, Groh A (2017) Multiplexed spike coding and adaptation in the thalamus. *Cell Rep* 19:1130–1140.
43. Oswald AM, Chacron MJ, Doiron B, Bastian J, Maler L (2004) Parallel processing of sensory input by bursts and isolated spikes. *J Neurosci* 24:4351–4362.
44. Panzeri S, Brunel N, Logothetis NK, Kayser C (2010) Sensory neural codes using multiplexed temporal scales. *Trends Neurosci* 33:111–120.
45. Ratté S, Hong S, De Schutter E, Prescott SA (2013) Impact of neuronal properties on network coding: Roles of spike initiation dynamics and robust synchrony transfer. *Neuron* 78:758–772.
46. Krüger J, Aiple F (1988) Multimicroelectrode investigation of monkey striate cortex: Spike train correlations in the infragranular layers. *J Neurophysiol* 60:798–828.
47. Tanaka H, Tamura H, Ohzawa I (2014) Spatial range and laminar structures of neuronal correlations in the cat primary visual cortex. *J Neurophysiol* 112:705–718.
48. Hong S, Ratté S, Prescott SA, De Schutter E (2012) Single neuron firing properties impact correlation-based population coding. *J Neurosci* 32:1413–1428.
49. Staude B, Rotter S, Grün S (2008) Can spike coordination be differentiated from rate covariation? *Neural Comput* 20:1973–1999.
50. Denker M, et al. (2011) The local field potential reflects surplus spike synchrony. *Cereb Cortex* 21:2681–2695.
51. Schwartz O, Pillow JW, Rust NC, Simoncelli EP (2006) Spike-triggered neural characterization. *J Vis* 6:484–507.
52. Gabbiani F, Metzner W, Wessel R, Koch C (1996) From stimulus encoding to feature extraction in weakly electric fish. *Nature* 384:564–567.